Airborne Measurements of Forest and Agricultural Land Surface Emissivity at Millimeter Wavelengths

Tim J. Hewison, *Member, IEEE*

***Abstract*—Passive microwave radiometers have been operated on an aircraft over the an area of Sweden, near Uppsala in September 1995 and March 1997 as part of the Northern Processes Experiment (NOPEX). Their measurements have allowed the calculation of the emissivity of boreal forest and agricultural land surfaces at 24, 50, 89, and 157 GHz over a range of incidence angles and polarizations. These results show consistent differences between dense forestry, where the emissivity is close to 1 and open land, where it is approximately 0.96. These differences are examined and a model is presented to parameterize these surfaces by use of a Debye-like effective permittivity and Fresnel's reflection coefficients. This will allow retrievals of atmospheric temperature and humidity profiles to be made by satellite microwave sounders, such as the advanced microwave sounding unit (AMSU) over similar land surfaces.**

***Index Terms*—Agriculture, emission, forestry, microwave radiometry, millimeter wave radiometry, soil, surfaces.**

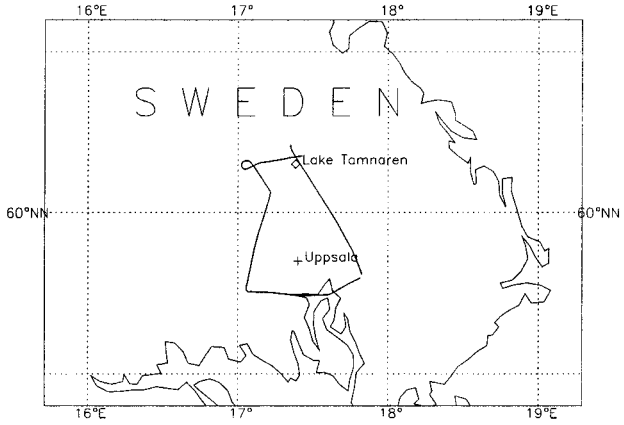

Fig. 1. Map of NOPEX area, showing typical flight track.

I. Introduction

THE LAUNCH of the next generation of satellite microwave instruments provides the opportunity to retrieve atmospheric temperature and humidity profiles over land as well as sea. English [1] has shown that an emissivity error of 0.02 or less is required to improve the accuracy of the lower tropospheric humidity analysis through variational assimilation of AMSU-B or SSM/T2 data. However, the analysis of lower tropospheric temperature over some land surfaces can be improved through assimilation of AMSU-A data using a specified emissivity of 0.95 [2]. Such applications require realistic representation of the surface's emissivity over 20–200 GHz and incidence angles between 0–50° by a fast parametric model [3].

This paper presents such a model and shows how it has been used to describe airborne measurements over forest and agricultural land surfaces. These measurements were made by the U.K. Meteorological Office (UKMO) over the Northern Processes Experiment (NOPEX) area, near Uppsala in Sweden.

This region, shown in Fig. 1, contains extensive areas of dense boreal forest dominated by spruce and pine, with about 15% deciduous broadleaf trees, as well as lakes, wetland and open agricultural land. The soil texture in the agricultural areas was described as "silt loam" or "silty clay loam," with an average of 26.8% clay and 17.0% sand [4].

The microwave emissivity of land surfaces depends on many factors. Emission is a function of the material's dielectric permittivity, structure, and temperature. Surface and volume scattering depend on its structure and permittivity. These processes occur in both the soil and vegetation canopy.

Many of the processes affecting surface emissivity at low frequencies (< 20 GHz) are now well understood, as a result of numerous ground-based airborne and satellite experiments. It has been shown that the emissivity of bare soil surfaces depends strongly on the soil moisture profile [5] and roughness [6], and weakly on the soil's structure [7]. It has also been found that the optical depth of vegetation depends on its water content and single scattering albedo [8]. This paper presents measurements between 24–157 GHz and investigates which of these processes influence the measured emissivities.

II. Proposed Model

Given the limited information available for modeling land surfaces on a scale appropriate for satellite retrievals, a fully physical emission model is not feasible. This paper describes a semi-empirical model for the emissivity of the surface/canopy system as a whole. The advantage of this model is its ability to predict the emissivity for land surfaces at any frequency between 20–200 GHz at arbitrary incidence angle and polarization based on only four empirically fitted parameters. This model has the additional advantage that it can also represent the sea surface emissivity, from which its parameters were originally defined. Its application to satellite retrievals is described in more detail in [3].

Manuscript received September 17, 1998; revised May 17, 2000. This work was supported in part by the Northern Processes Experiment (NOPEX; a northern hemisphere climate processes land-surface experiment) and Scientific Training and Access to Aircraft for Atmospheric Research Throughout Europe (STAAARTE), which is funded by the European Commission through the Training and Mobility of Researchers (TMR) Program.

The author is with the Meteorological Office, Hants, GU14 0LX U.K. (e-mail: tjhewison@meto.gov.uk).

Publisher Item Identifier S 0196-2892(01)01176-7.

The surface can be represented in terms of a specular reflector, based on a Debye-like form of effective relative permittivity ε at frequency ν, which is parameterized in terms of ε_s, the effective static permittivity ε_∞, its high frequency limit, and ν_r, the effective relaxation frequency. The ionic conductivity term has been neglected, as its contribution is insignificant above 20 GHz

$$\varepsilon(\nu) = \frac{\varepsilon_s - \varepsilon_\infty}{1 - i.\nu/\nu_r} + \varepsilon_\infty. \tag{1}$$

The Fresnel formulae below define the power reflectivity in vertical and horizontal polarizations Γ_v and Γ_h of a specular surface in terms of its complex relative permittivity, ε and the angle of incidence θ. The emissivity (e) is the complement of this [$e(\nu, \theta) = 1 - \Gamma(\nu, \theta)$]

$$\Gamma_v(\nu, \theta) = \left| \frac{-\varepsilon(\nu)\cos\theta + \sqrt{\varepsilon(\nu) - \sin^2\theta}}{\varepsilon(\nu)\cos\theta + \sqrt{\varepsilon(\nu) - \sin^2\theta}} \right|^2$$

OR

$$\Gamma_h(\nu, \theta) = \left| \frac{\cos\theta - \sqrt{\varepsilon(\nu) - \sin^2\theta}}{\cos\theta + \sqrt{\varepsilon(\nu) - \sin^2\theta}} \right|^2. \tag{2}$$

Such a scheme can represent emissivity that increases with frequency by setting $\varepsilon_s > \varepsilon_\infty$. Conversely, emissivity decreasing with frequency, can be represented by $\varepsilon_s < \varepsilon_\infty$. However, surfaces exhibiting nonmonotonic emissivity spectra, such as dry snow [9], cannot be accurately represented without the addition of a scattering term. It is proposed that the effects of variable surface roughness and vegetation cover are absorbed into the three parameters (ε_s, ε_∞, ν_r) of Debye's formula (1), though this will be further discussed later.

Bragg scattering by small-scale surface roughness was modeled by Choudhury *et al.* [6] by scaling the surface reflectivity by an exponential factor of a roughness parameter $h' = (4\pi\nu\sigma/c)^2$ where σ is the root mean square (rms) height of the surface

$$e_p(\nu, \theta) = 1 - \Gamma_p(\nu, \theta)e^{-h'\cos^2\theta}. \tag{3}$$

However, such a formulation does not take into account the fact that the surface correlation length is typically much larger than the rms roughness when measured at a scale appropriate for millimeter wavelengths. To allow for this, the roughness parameter is often regarded as a free parameter for a given surface, independent of frequency.

Geometric optics can be used to give a more realistic representation of surface roughness by calculating the reflectivity for a myriad of surface facets, assuming a gaussian slope distribution. However, this is too computationally expensive for use in operational retrievals.

An additional parameter for polarization mixing Q was added by Wang and Choudhury [10] and is included in the proposed model to reproduce the observed angular variation of emissivity

$$\Gamma'_h = (1 - Q)\Gamma_h + Q\Gamma_v$$

OR

$$\Gamma'_v = (1 - Q)\Gamma_v + Q\Gamma_h. \tag{4}$$

Although roughness is not treated explicitly in the model, its effects are included in the effective permittivity and polarization mixing parameters. This is done because roughness cannot be suitably quantified on the global scale needed for the model's intended use.

Most vegetation (except when very sparse, short, or dry) appears optically thick at millimeter wavelengths due to absorption and volume scattering within the canopy. The effective emissivity is then determined by the vegetation's single scattering albedo: the ratio of its volume scattering to extinction coefficients [8], which are frequency dependent. Again, due to the inadequacy of quantitative vegetation information, this process is also absorbed into the effective permittivity and polarization mixing parameters. The effective surface temperature is that of the vegetation as measured by thermal infrared radiometry.

III. Measurements

A. Instrumentation

This paper presents measurements made by the UKMO on the C-130 Hercules. The main instruments used in this study are the microwave radiometers, known as Deimos and microwave airborne radiometer scanning system (MARSS). These are total power radiometers both with a 3 s along-track scan, which includes various views downward (and upward for MARSS) and two onboard black body calibration targets. These instruments are described in full in [11], [12]. Table I summarizes their performance at low-level over land during the September phase of this experiment. The absolute accuracy of the brightness temperatures were estimated with reference to scenes of known radiance. These figures were about 25% better in March due to the improved thermal contrast between calibration targets.

The UKMO aircraft also operated a range of meteorological and navigational instrumentation useful to the analysis of the data. These include air temperature, humidity, pressure, windspeed, surface temperature (from a thermal infrared radiometer—8–15 μm, with a 2.0° field of view), and hemispherical fluxes in three bands (from upper and lower pyranometers at 0.3–3.0 μm, 0.7–3.0 μm, and pyrgeometers at 4–50 μm), GPS position, and radar altitude.

The scanning airborne filter radiometer (SAFIRE) was also operated during the March 1997 flights. This recorded shortwave radiances at 0.62 μm and 0.87 μm, with a 2.6° field of view, which were used to provide a vegetation index. However, the most useful instrument for identification of surface conditions was the downward facing video camera.

B. Flights

One flight was made on September 6, 1995 on a warm day after heavy rain. Two further flights took place on March 14 and 18, 1997 in much colder conditions. Each flight comprised three or four circuits of straight, level runs around the area at altitudes of 150, 300 and 600–900 m above ground level. The track of one such circuit is plotted on the map in Fig. 1. Each circuit takes

TABLE I
SUMMARY OF UKMO MICROWAVE RADIOMETER SYSTEMS

Instrument	Deimos		MARSS	
Frequency /GHz	23.8	50.1	89.0	157.0
View angles	+35° to -5° Down only		+40° to -40° Up and Down	
Scan period	3s		3s	
Beamwidth (3dB)	11°		11°	
Polarisation	V&H	V&H	Mixed	V or H
Integration time	50ms	50ms	80ms	80ms
Sensitivity, ΔT	0.6K	0.6K	0.3K	0.5K
Accuracy	1.5K	1.5K	0.9K	0.8K

TABLE II
WEATHER OBSERVATIONS AT UPPSALA

Date	T_{min}	T_{max}	Precip
4/9/95	+12.3°C	+15.0°C	22mm
5/9/95	+11.7°C	+15.3°C	11mm
6/9/95	+11.9°C	+22.3°C	0.2mm
13/3/97	+2.1°C	+9.4°C	0.1mm
14/3/97	-4.0°C	+2.6°C	nil
15/3/97	-6.1°C	+3.5°C	0.2mm
16/3/97	-5.6°C	+1.4°C	nil
17/3/97	-11.0°C	+1.0°C	nil
18/3/97	-8.8°C	+1.1°C	nil

approximately 35 m to complete at an average ground speed of 90 m/s.

C. Weather

Weather observations from Uppsala, Sweden, are given in Table II. The first flight on September 6, 1995, followed two days of heavy rain, so soil moisture may be assumed to be very high, though no standing water was evident in the fields. During the period of the second visit, the nighttime minima decreased following the passage of a cold front on March 13, 1997, which brought light precipitation. The surface remained snow-free throughout. Daytime air temperature climbed above 0° C each day, causing the frozen surface to thaw a little.

Shallow convective cloud formed during the afternoon of all three flights.

IV. EMISSIVITY CALCULATION

Measured brightness temperatures must be converted to surface emissivity to extend them to general application. The following formula is used to calculate the emissivity using only aircraft data

$$e(\nu, \theta) = \frac{T_n(\nu, \theta) - T_z(\nu, \theta)}{T_S - T_z(\nu, \theta)} \tag{5}$$

where

- e emissivity at frequency ν and incidence angle θ;
- T_n and T_z upwelling and downwelling brightness temperatures at the surface;
- T_S surface's skin temperature.

Downwelling brightness temperatures at Deimos's frequencies are predicted from the MARSS observations. Corrections are then applied for absorption below the aircraft, based on radiative transfer model calculations of the atmospheric transmittance. The stages involved in the emissivity calculation are described in full in [9]. The emissivity calculation assumes cloud-free conditions, so data is rejected where the downwelling brightness temperatures measured by MARSS were above a threshold consistent with clear air.

The skin temperature of the surface T_S was measured by the aircraft's thermal infrared radiometer, assuming an infrared emissivity of one ($e_{ir} = 1.00$). A more realistic value of $e_{ir} = 0.982$ for water or crop-land results in a small bias of $+\,0.002$ on a retrieved microwave emissivity of $e_{mw} = 0.95$ under clear winter skies. Such a skin temperature is typical of those available to retrieval schemes for satellite data and provides a good proxy for the temperature for surface emissions, as penetration depths are very small ($\leq$ 10 mm) at millimeter wavelengths.

The absolute accuracy of emissivity is calculated by considering the uncertainty in each of the terms in (5). This is approximately $\pm\,0.007$ for $e = 0.950$ for each channel, except 157 GHz in September, which is $\pm\,0.011$ due to the high downwelling brightness temperatures. This is dominated by uncertainties in upwelling brightness temperatures.

V. ANALYSIS BY VIDEO CLASSIFICATION

Footage from the aircraft's downward-facing video camera was studied to identify periods during which homogeneous surface types were overflown. A category was assigned to each sample according to the vegetation type and density, and surface temperature. "Open" refers to canopy cover between 30–70%; "Close" refers to canopy cover greater than 70%. From the three flights, 142 samples were identified in this way, with periods ranging from 10–50 s, corresponding to track lengths of 1–5 km.

A. Nadir Emissivity Spectra

The emissivity was calculated for each of these samples in the view nearest to nadir. Fig. 2 shows the near-nadir emissivity spectra of the categories. The points show the mean and standard deviation of each sample. The spectrum of each sample is illustrated by a dashed line. The solid lines represent curves fitted by selection of the three parameters of the Debye formulation (1) of effective permittivity. The mean nadir emissivities are reproduced in Table III.

Open Water was observed in the fresh water lake, Tämnaren, which was calm (10 m windspeed $<$ 1.5 m/s) on all three flights. This is compared to the specular emissivity predicted by the measurements of sea water permittivity reported by Guillou *et al.* [13], using a "double-Debye" model. The sensitivity to salinity is minimal above 20 GHz, and can be neglected. Further comparisons with this model are made in the following section on angular dependence.

During March 1997, Lake Tämnaren partially froze over. The *Lake Ice* category included six samples of ice of various thickness (the fitted data is calculated using only the four thickest samples.). Pure ice greater than 0.2 m thick can be regarded as an infinite dielectric slab and has a flat emission spectra at frequencies above 20 GHz [9].

Bare Soil was subdivided into two categories according to its surface temperature. If $T_S < 0°$ C, it was classified as frozen.

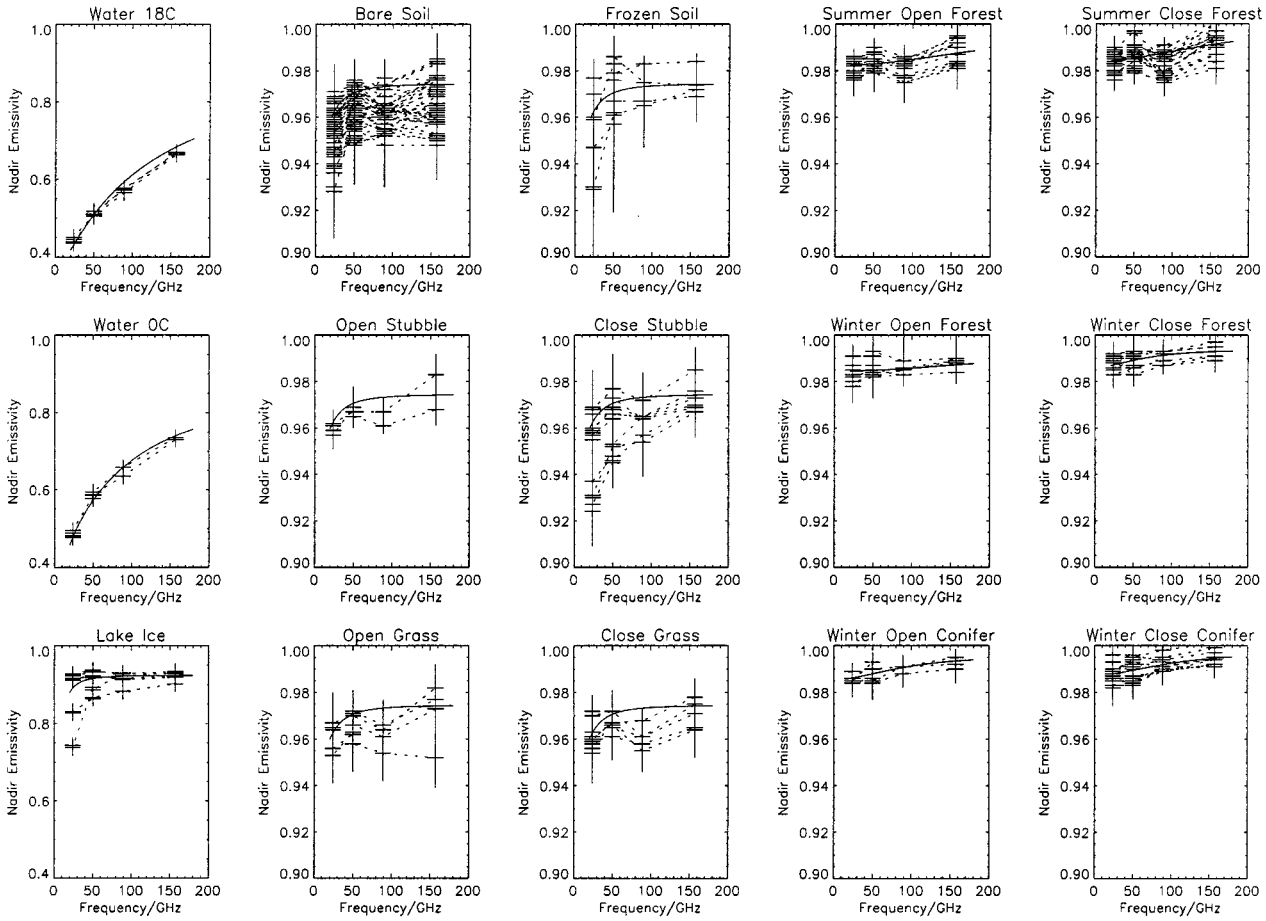

Fig. 2. Nadir emissivity spectra for categories identified by video. All samples within each surface category are shown, linked with dashed lines, and error bars representing standard error of mean. Continuous lines show the models for sea water from Guillou *et al.* [13] and this paper for other surfaces.

TABLE III
MEAN NADIR EMISSIVITIES FOR VIDEO CLASSIFICATIONS

Category	$e(24)$	$e(50)$	$e(89)$	$e(157)$
Water 18C	0.443	0.513	0.573	0.668
Water 0C	0.491	0.588	0.657	0.733
Lake Ice	0.908	0.920	0.922	0.925
Bare Soil	0.955	0.967	0.962	0.966
Frozen Soil	0.962	0.982	0.979	0.980
Open Stubble	0.960	0.966	0.962	0.974
Close Stubble	0.953	0.963	0.962	0.974
Open Grass	0.959	0.968	0.961	0.973
Close Grass	0.964	0.967	0.963	0.972
Summer Open Forest	0.983	0.985	0.983	0.990
Summer Close Forest	0.984	0.987	0.985	0.994
Winter Open Forest	0.985	0.986	0.985	0.987
Winter Close Forest	0.987	0.990	0.991	0.993
Winter Open Conifer	0.987	0.989	0.991	0.994
Winter Close Conifer	0.989	0.990	0.992	0.995

Both showed a wide range of emissivity, which is investigated in Section VI-B.

Stubble and *Grass* were only observed in September 1995 and were not extensive. No consistent differences are apparent between these categories and bare soil, which may due to the vegetation scattering signal being of the same order as the soil's reflected signal. This is further investigated in Section VI-A.

Summer Forest includes some in-leaf deciduous areas, which were not differentiable from conifers on the video footage. *Winter Forest* included a mix of about 80% coniferous and 20% leafless deciduous trees. Those areas that could be confirmed as purely coniferous were given the classification *Winter Conifer*, and showed even higher emissivity due to a lower single scattering albedo. These results are consistent with modeling work at lower frequencies [14], which suggested lower emissivity for deciduous forestry due to reflections from the leaves' flat surfaces.

B. Emissivity Variation with Incidence Angle

Fresnel's equations can predict a surface's specular reflectivity in two orthogonal polarizations over a range of view angles from its effective permittivity. This is an important feature of this scheme, as it allows representation over the range of view angles and polarizations observed by a cross-track scanning satellite instrument.

Both of Deimos's channels measure two polarizations, which rotate with scan angle so as to measure vertical and horizontal in the forward view ($+35°$). However, there is evidence from measurements over open water that the horizontal polarization of the 50 GHz channel is somewhat misaligned causing the polarization contrast to be underestimated.

MARSS's channels measure only one polarization in each of its nine downward views. This polarization rotates with scan angle. The polarization of the 157 GHz channel rotates from

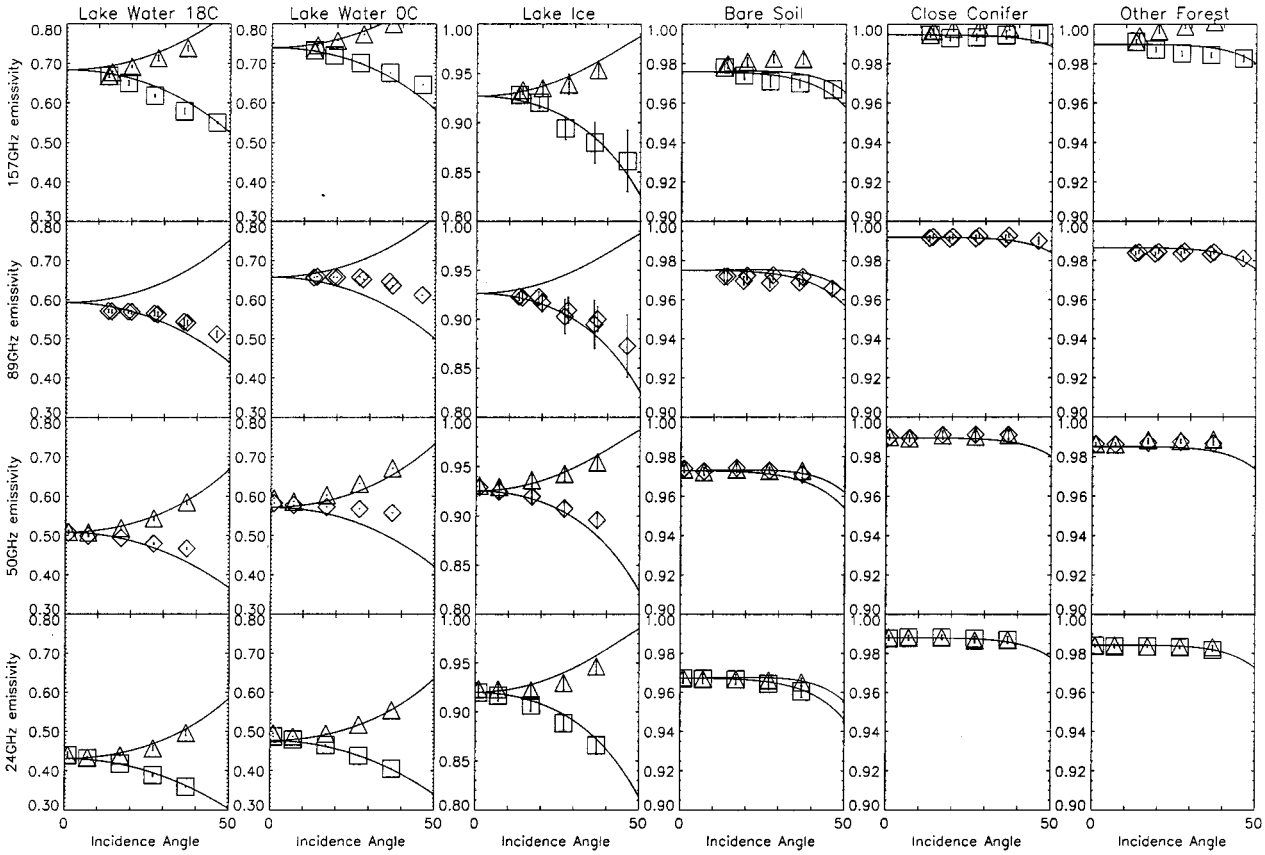

Fig. 3. Average emissivity of all samples within each surface category identified by video. Graphs are shown for all observed frequencies at all incidence angles. Symbols represent observed polarization: △ = Vertical, □ = Horizontal, ◇ = Intermediate. Continuous lines show the models for sea water from Guillou *et al.* [13] and this paper for other surfaces.

horizontal in the $+20°$ view to vertical at $-40°$. The polarization of the 89 GHz channel also rotates but only approaches horizontal in the nadir view and is intermediate at the scan extremes.

Emissivity curves were calculated for each of the samples identified from video, grouped into radiometrically resolvable categories. Fig. 3 shows the mean and standard error of the emissivity measured in each view. The lines show the proposed model based on parameters fitted to these data.

The calm *Lake Water* behaves as a specular surface, closely following the double-Debye model described by Guillou *et al.* [13] shown by the continuous curves. However, grease ice was present in March 1997, so these results should not be taken as significant validation of the permittivity models. Note the small bias evident in these curves at low incidence angles ($< 10°$), due to reflection of the aircraft in the surface. Care should therefore be taken when interpreting the significance of nadir emissivity spectra such as those shown for open water in Fig. 2. However, this effect is insignificant for land surfaces with lower nonspecular reflectivity.

Lake Ice also exhibits specular behavior, though the bias at low incidence angles is smaller. The apparent decrease in the ice's emissivity at 24 GHz may be attributable to the fact that it was not sufficiently thick to be treated as an infinite dielectric slab. However, its thickness was not measured, so it is not possible to model it as a finite layer over water. Note the large error bars on the MARSS (89 and 157 GHz) data for this group, due to the difficulty of comparing view angles over short sample periods.

Bare Soil has a high emissivity with very little polarization contrast. *Grass* and *stubble* are not shown here, but exhibited very similar spectra and angular variations. Such behavior cannot be explained by small-scale roughness using a simple model, such as that of Choudhury [6], as this implies the emissivity tends to one as the roughness increases. A geometric optics model could reproduce these results, but is too computationally expensive for use in operational satellite retrievals.

Close Conifer Forest was observed in March 1997 and shows very high emissivity at all frequencies, with no polarization difference, due to the large optical depth of the canopy and its low single scattering albedo.

Other Forest combined all remaining forest categories observed in summer and winter. The average canopy density of this group was somewhat lower, exposing some bare soil and rocky outcrops, resulting in a decrease in emissivity, especially at the lower frequencies.

VI. Analysis by LANDSAT Classification

To further investigate the dependence of the surface's emissivity on various parameters describing its condition, it was necessary to use more extensive datasets. These were provided by a land-use classification map of the NOPEX area. This approach

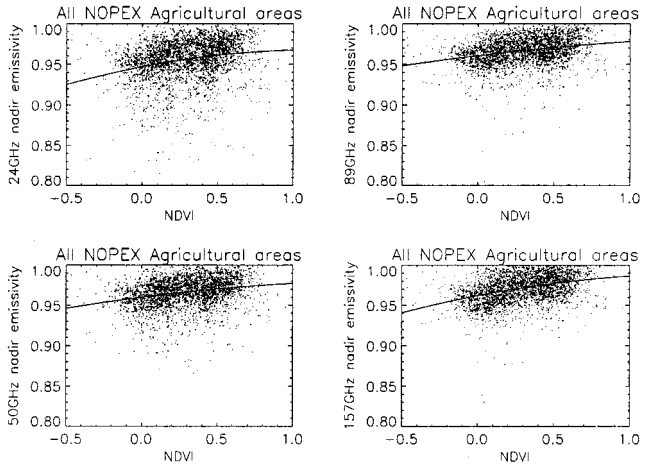

Fig. 4. Effect of vegetation cover (as NDVI) on emissivity of at 24, 50, 89, and 157 GHz of all unfrozen agricultural areas based on LANDSAT classifications.

provides an analytic tool with different benefits and drawbacks to the categories assigned manually from video footage in Section V-A.

This land-use map was based on the classification of LANDSAT TM 2345 (Date 890 707), merged with Swedish National Land Survey's (LMV) "Roda Kartan" map data for forest, wetland and built-up areas. This map has been filtered with a 7×7 mode filter to generalize into 200 m pixel size. A land-use classification has been assigned to each second of data, according to the aircraft's position, measured by a Navstar XR5 global positioning system (GPS) receiver.

Although this map is based on an old satellite overpass, it is believed to be reasonably accurate, as forest clear-cutting is not common in this area. Its major inadequacies are in agricultural areas. To overcome this, the agricultural land-use classifications were combined, and re-classified according to the normalized difference vegetation index (NDVI).

For the September 1995 flight, NDVI is calculated from the ratio of fluxes measured by the aircraft pyranometers, with clear (0.3–3.0 μm) and red (0.7–3.0 μm) filters. For the March 1997 flights, these instruments were less reliable, and the SAFIRE radiometer was available, allowing NDVI to be calculated from its shortwave channels (0.62 μm and 0.87 μm)

$$\mathrm{NDVI} = \frac{S_{0.87\ \mu\mathrm{m}} - S_{0.62\ \mu\mathrm{m}}}{S_{0.87\ \mu\mathrm{m}} + S_{0.62\ \mu\mathrm{m}}}$$

or

$$\mathrm{NDVI} = \frac{S_{red} - (S_{clear} - S_{red})}{S_{red} - (S_{clear} - S_{red})}. \tag{6}$$

The NDVI derived from both instruments was found to behave in a similar way, ranging from -0.30 for open water to $+0.60$ for dense forest. However, the slow response of the pyranometers meant their NDVI could only be used for the lowest altitude runs (150 m) to ensure fields of view were compatible with that of the microwave radiometers. The NDVI calculated in this way for each second of aircraft data was used to filter the land-use classifications, especially to resolve bare soil from vegetated agricultural land.

Further filtering is applied to remove periods which may be contaminated by inhomogeneous clouds in the upward views and aircraft turns. After filtering, approximately 4% of samples classified as "open water" produced microwave emissivities incompatible with this classification [i.e., $e(24\ \mathrm{GHz}) > 0.5$]. The remainder are in good agreement with those in Section V-A.

A. Influence of Vegetation

The extensive dataset provided by combining the aircraft data with the land-use map allows us to investigate the cause of the large variation in emissivity over agricultural land. Fig. 4 shows the nadir emissivity and NDVI of the combined agricultural land-use classifications (bare soil, crops and pastures), where the surface temperature is greater than 0° C. Also included are lines representing quadratic fits to these data. The influence of vegetation is clear at the higher frequencies, increasing the emissivity due to absorption and scattering within the canopy. However, the extra spread at 24 GHz suggests another mechanism is present at this frequency.

From Fig. 4, values for mean nadir emissivity of "bare soil" and "crops" were extracted for observations with surface temperature greater than $+4°$ C and NDVI within 0.05 of $+0.05$ and $+0.60$, respectively. Similarly, values for "frozen soil" were calculated when $T_S < 0°$ C and $0.00 < \mathrm{NDVI} < +0.10$. Values for these classes were used to calculate model coefficients as described in Section VII.

B. Influence of Soil Moisture and Frozen Soils

Some of the observed variation in the emissivity of bare soil may be due to differences in soil moisture along the flight track. The addition of liquid water to the soil particle/water/air mixture will increase its permittivity, and decrease the emissivity, especially at lower frequencies. Although the soil moisture was believed to be high during the flights, changes in meteorological and hydrological conditions will cause it to vary across the area. However, ground truth measurements were not available at a sufficient resolution to analyze this effect. In the future, it may be possible to further refine the model by parameterizing its effective static permittivity, ε_s, in terms of the soil moisture.

Another possible cause of the variation in the emissivity of bare soil could be partially frozen soil. This is expected to have a higher emissivity due to the relatively low permittivity of ice compared with liquid water. No equivalent effect is expected (or observed) for the NDVI, as neither liquid water or ice have absorption features at these wavelengths (0.62 μm or 0.87 μm). The nadir emissivity of the "Bare Soil" classification is plotted against the surface temperature measured by the aircraft's thermal infrared radiometer in Fig. 5, for the winter flights.

At high frequencies, the emissivity is found to be higher for frozen soil than in unfrozen areas, as expected. The transition between frozen and unfrozen ground is gradual, due to the effects of solar insolation on the surface layers, and the localized shadowing that occurs at these low solar angles. However, there is more spread evident at the lower frequencies. This is believed to be due to the increased sensitivity of these channels to surface water, presumably formed when frozen areas thaw during the day.

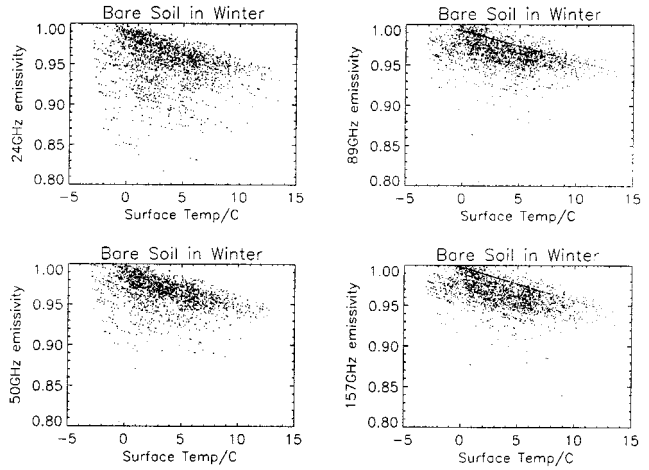

Fig. 5. Effect of surface temperature on emissivity of bare soil at 24, 50, 89, and 157 GHz based on LANDSAT classifications and NDVI filtering.

VII. Fitting Model Parameters to Observations

Coefficients of effective permittivity (ε_s, ε_∞, ν_r) were fitted by least squares regression to average emissivities measured at nadir for various land-use classifications, derived from one or other classification techniques. Video-based classifications of *water* and *lake ice* were kept, whilst those of all forest types were combined as *forest*, except *close conifer*, measured in winter. However, figures for *bare soil*, *frozen soil*, and *close crops* were calculated from data analyzed by the technique described in Section VI. The polarization mixing parameter, Q, was taken from the fits used in Fig. 3. Table IV shows the results.

The model was found to fit the samples of emissivity at nadir shown in Fig. 2 with an rms error of 0.009 for bare soil, close crops and water and 0.004 for forest. This is well within the requirement for retrieving humidity information over these surfaces [1].

Curiously, 157 GHz shows the largest polarization differences over most NOPEX land types observed. However, this effect is believed to be caused by an intermittent systematic error in the instrument, introducing a view dependence at 157 GHz as a result of changing geometry in the optical path, producing internal standing waves. The calibration was only validated at the nadir and zenith positions, where it is believed to be accurate to ± 1 K for brightness temperatures of 250 K. It cannot be concluded the polarization mixing is frequency dependent, so Q was fitted using only the reliable polarization data measured at 24 GHz.

VIII. Conclusions

This paper has presented the measurements of boreal forest and agricultural land in Sweden by airborne microwave radiometers. They have allowed the development of a fast, parametric model capable of representing the emissivity of these surfaces over the range of frequencies and view angles needed for the next generation of satellite sounding instruments.

The model presented is based on a three-parameter Debye formulation of effective permittivity, and Fresnel's equations. It can predict the variation of emissivity with frequency from 20–200 GHz. However, an additional polarization mixing parameter is necessary to represent the observed decrease in polarization contrast over land surfaces.

Low level aircraft data was analyzed by classifying the surface type by two independent techniques, producing consistent emissivity spectra. The emissivity was found to correlate with vegetation cover, offering the possibility of parameterizing all these land types in terms of a single vegetation parameter. It was also found to depend on surface temperature, as a result of the freezing of the water in the soil's dielectric mixture.

Model coefficients were calculated for groups of these land-use classifications by fitting observed nadir emissivities to the Fresnel–Debye functions. This model was able to fit the observed emissivity of bare soil and crops with an rms accuracy of 0.009 and forestry with an accuracy of 0.004. This is sufficient to allow retrieval of some information on lower tropospheric humidity from the advanced microwave sounding unit (AMSU) over land [1].

TABLE IV
Model Coefficients of Effective Permittivity

	Permittivity Coeffs			Depol.
Category	ε_s	ε_∞	ν_r/GHz	Q
Lake Ice	40.8	3.03	0.44	0.00
Bare Soil	2.64	2.25	63.6	0.40
Frozen Soil	2.22	1.64	51.9	0.40
Close Crops	2.20	1.94	67.4	0.42
Winter Close Conifer	1.57	1.22	87.3	0.50
Other Forestry	1.66	1.01	163.0	0.50

Acknowledgment

The author would like to thank the organizers of NOPEX, especially T. Persson for supplying the LANDSAT map and S. English for his comments on this paper. The author would like to acknowledge the support of the ground and air crew of the Royal Air Force, the scientists and technicians of the Meteorological Research Flight, especially D. Kindred for coordinating a second campaign in the NOPEX area under the auspices of the Scientific Training and Access to Aircraft for Atmospheric Research Throughout Europe (STAAARTE).

References

[1] S. J. English, "Estimation of temperature and humidity profile information from microwave radiances over different surface types," *J. Appl. Meteorol.*, vol. 38, no. 10, pp. 1526–1541, 1999.

[2] S. J. English, R. J. Renshaw, P. C. Dibben, A. J. Smith, P. J. Rayer, C. Poulsen, R. W. Saunders, and J. R. Eyre, "A comparison of the impact of TOVS and ATOVS satellite sounding data on the accuracy of numerical weather forecasts," *Q. J. R. Meteorol. Soc.*, to be published.

[3] S. J. English and T. J. Hewison, "A fast generic millimeter-wave emissivity model," *Proc. SPIE*, vol. 3503, pp. 288–299, 1998.

[4] J. F. de Ruiter and A. A. van de Griend, "Analysis of air borne passive microwave measurements for vegetation and soil moisture monitoring," Inst. Earth Sciences, Vrije Univ., De Boelelaan 1085, NL-1081 HV, Amsterdam, The Netherlands, NOPEX Tech. Rep. 22, 1996.

[5] R. W. Newton and J. W. Rousse, "Microwave radiometer measurements of soil moisture content," *IEEE Trans. Antennas Propagat.*, vol. AP-28, pp. 680–685, May 1980.

[6] B. J. Choudhury, T. J. Schmugge, A. Chang, and R. W. Newton, "Effect of surface roughness on the microwave emission from soils," *J. Geophys. Res.*, vol. 84, no. C9, pp. 5699–5706, 1979.

[7] T. J. Schmugge, "Effect of texture on microwave emission from soils," *IEEE Geosci. Remote Sensing*, vol. GE-18, pp. 353–361, May 1980.
[8] A. A. van de Griend and M. Owe, "Microwave vegetation optical depth and inverse modeling of soil emissivity using Nimbus/SMMR satellite observations," *Meteorol. Atmos. Phys.*, vol. 54, pp. 225–239, 1994.
[9] T. J. Hewison and S. J. English, "Airborne retrievals of snow and ice surface emissivity at millimeter wavelengths," *IEEE Trans. Geosci. Remote Sensing*, vol. 37, pp. 1871–1879, July 1999.
[10] J. R. Wang and B. J. Choudhury, "Remote sensing of soil moisture content over bare field at 1.4GHz frequency," *J. Geophys. Res.*, vol. 86, pp. 5277–5282, 1981.
[11] T. Hewison, "The design of deimos: A microwave radiometer with channels at 23.8G Hz and 50.3G Hz for the UK Met. research flight C-130 aircraft," in *Proc. Int. Geoscience and Remote Sensing Symp.'95*, 1995, pp. 2261–2263.
[12] S. J. English, C. Guillou, C. Prigent, and D. C. Jones, "Aircraft measurements of water vapor continuum absorption," *Q. J. R. Meteorol. Soc.*, vol. 120, pp. 603–625, 1994.
[13] C. Guillou, W. Ellison, L. Eymard, K. Lamkaouchi, C. Prigent, G. Delbos, G. Balana, and S. A. Boukabara, "Impact of new permittivity measurements on sea surface emissivity modeling in microwaves," *Radio Sci.*, vol. 33, pp. 649–667, 1998.
[14] P. Ferrazzoli and L. Guerriero, "Passive microwave remote sensing of forests: A model investigation," *IEEE Trans. Geosci. Remote Sensing*, vol. 34, pp. 433–443, Mar. 1996.

Tim J. Hewison (M'97) received the B.Sc. (Hons.) degree in physics with astrophysics from the University of Manchester, Manchester, U.K., in 1989, and the M.Sc. degree in meteorology from the University of Reading, Reading, U.K., in 1999.

Since 1990, he has been with the Remote Sensing branch of the U.K. Meteorological Office. His work has included the analysis of AMSU-B radiometric and antenna tests and the development of microwave radiometers for the U.K. Meteorological Office C-130 research aircraft. He has conducted and analyzed a series of aircraft experiments to measure the microwave emissivity of various surface types, the subject of his M.Sc. thesis. He is also a Member of COST Action 712 on the application of microwave radiometry to atmospheric research.